Simulating Dipole-dipole Interactions on the Hyperkagome Lattice, A New Spin Ice

by

Travis E. Redpath

A Thesis submitted to the Faculty of Graduate Studies of

The University of Manitoba

in partial fulfillment of the requirements of the degree of

MASTER OF SCIENCE

Department of Physics and Astronomy

University of Manitoba

Winnipeg

Abstract

Motivated by studies of non-magnetic dopings of pyrochlore spin ice and the experimental realization of the hyperkagome lattice in $Na_4Ir_3O_8$(38), this work studies the dipolar ice model on the hyperkagome lattice. This is a local $< 111 >$ Ising model with classical spins featuring an antiferromagnetic neighbour exchange as well as a long range dipolar interaction, previously studied on the pyrochlore lattice(18). A hybrid single spin flip/loop algorithm Monte Carlo code has been developed to address ergodicity issues seen at low temperatures. This algorithm agrees with analytical results for the smallest system size and has been extended to larger system sizes. A phase diagram very similar to that of the pyrochlore lattice(19) is found with an antiferromagnetic region as well as regions with a spin ice crossover and a low temperature ordering transition. An additional charge-ordered state, similar to that in the recently studied kagome spin ice(11), was also found.

Acknowledgements

This work has been supported by a University of Manitoba Graduate Fellowship. I'd like to thank my advisor Dr. John Hopkinson and my advisory committee members Dr. Byron Southern and Dr. Chris Wiebe. Also, Dr. Matthew Enjalran and Patrick Carter for their work on the Ewald summation.

Table of Contents

List of Tables

List of Figures

Chapter I: Introduction

In this thesis we will be concerned with properties of spin, interactions between spins, and how these interactions can become frustrated. The field of geometrically frustrated systems has been around since Pauling's(1) proposal in 1935 that the structure of cubic water ice allowed for many equivalent ways of satisfying the ice rules that had been previously defined by Bernal and Fowler(2). Quantum spin liquids are an extension of this where quantum spins, instead of the hydrogen atoms from water ice, remain disordered to very low temperature. Quantum spin liquids were described by Anderson(3) using a resonating-valence-bond theory where pairs of spins become entangled due to an antiferromagnetic interaction and act as a single entity with 0 spin. Investigations into quantum spin liquids continues to be very active and only recently(4) has experimental evidence for their existence been seen. Until 1986 it was thought that magnetism was detrimental to superconductivity. This was proven incorrect with the discovery of superconductivity in a magnetic material(5) which also had a critical temperature much higher than had previously been seen giving birth to the field of high temperature superconductivity. Anderson extended his resonating-valence-bond theory to propose an explanation for this phenomenon(6) as dopings in the lattice allowing the charged, spinless pairs to move and superconduct. These recent findings in the fields of quantum spin liquids and high temperature superconductors have not only invigorated the search for and research on frustration in quantum systems but also in their classical analogs such as Ising spin systems, also known as spin ices, as will be presented here.

Spin

Spin is a quantum version of angular momentum which does not have anything to do with actual spinning. When current is run through a loop of wire or an electrically charged object is spinning a magnetic field is produced. Macroscopically this magnetic field is identical to that of traditional bar magnet (Fig. 1a) with the direction of the magnetic moment the same as what the angular momentum vector would be if the atom was spinning (Fig. 1b). Spin as used in this sense is an

intrinsic property of the electrons of an atom similar to its charge or mass. Attempts to calculate the speed if the electrons of the atom were actually spinning using their size, charge, and the magnitude of the resulting magnetic field leads to speeds greater than that of the speed of light.

These spins can interact with each other through either a ferromagnetic (FM) or antiferromagnetic (AFM) interaction. A ferromagnetic interaction will cause the spins to favour aligning their magnetic moment in the same direction as their neighbours. In an antiferromagnetic interaction the interacting spins' magnetic moments will favour pointing in opposite directions.

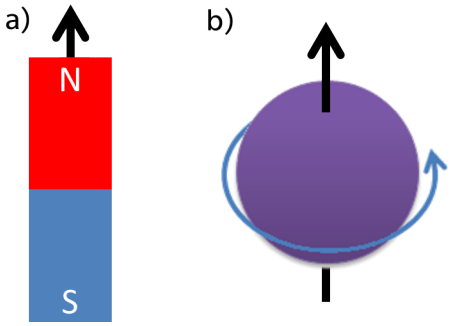

Figure 1: a) A bar magnet with the direction of its magnetic moment indicated by an arrow. b) An atom which has an intrinsic spin displays a magnetic moment similar to (but much smaller than) that of a bar magnet. Ferromagnetic interactions between atomic spins lead to macroscopic magnetic moments like those of a bar magnet.

Geometric Frustration

One of the first geometrically frustrated systems to be studied was the cubic form of water ice, whose hydrogen atoms form slightly distorted tetrahedra around each oxygen atom. In water ice each oxygen atom is surrounded by four hydrogen atoms. Two of them are close to the oxygen and form the polar water molecule and two of are further away and belong to neighbouring water molecules (Fig. 2). The neighbouring water molecule's hydrogen atoms form hydrogen bonds with the first oxygen atom. It was noted by Linus Pauling in 1935 that this configuration would result in water ice having a non-zero residual entropy(1). The following year Giauque and Stout(7) published measurements of the heat capacity of water ice down to 13K and used this measurement along with the Debye function for lower temperatures to compute a residual entropy that was in

close agreement with that estimated by Pauling.

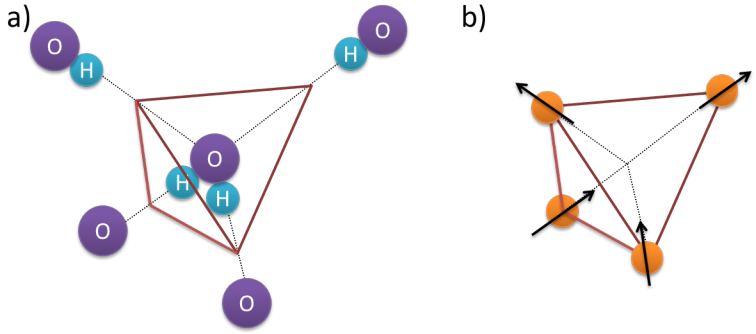

Figure 2: a) Water Ice with two hydrogen atoms sitting closer to the central oxygen atom and two sitting further away(1). b) The equivalent spin system to the cubic water ice with magnetic atoms at the corners of the tetrahedra that have spins pointing either towards the centre of the tetrahedra or away from it.

Unlike water ice, spin systems don't have atoms that move further from or closer to the centre of the tetrahedra. Instead, in some special materials magnetic atoms lying at the corners of tetrahedra have spins which are restricted to lie in one of two directions. Analogous to the displacement of the hydrogen atoms of water ice those directions point either towards the centre of the tetrahedra or directly away from it. This two state model is known as the Ising model.

Pauling's work was extended by Harris *et al.*(8) to describe an effective FM interaction between neighbouring spins on the pyrochlore lattice of $Ho_2Ti_2O_7$ with spins that have an Ising anisotropy directed along the local $<111>$ directions (which point toward or away from the centres of each corner-shared tetrahedron). In describing their work Harris *et al.* coined the terminology "spin ice". In the pyrochlore lattice instead of having atoms closer or further from the centre of a tetrahedron there were spins that either pointed towards the centre of the tetrahedron or away. In the ground state pyrochlore spin ice is forced to obey similar rules to water ice with two of those spins oriented away from the centre of the tetrahedron and two oriented towards it as discussed in the context of geometric frustration.

The ground state of the outer f-electrons of the rare earth atoms is highly anisotropic favouring two opposing directions. The first group of excited states in spin ice materials lies well above the ground state. The first excited states of $Ho_2Ti_2O_7$ and $Dy_2Ti_2O_7$(9) occur at 237K and 383K,

respectively. The temperatures discussed in this thesis are well below the temperatures of the first excited states so those states are considered unreachable in this work. This strong anisotropy constrains the magnetic moments to behave as Ising spins with their direction aligned with the local $<111>$ axis. For the pyrochlore lattice the local $<111>$ directions connect the centres of the two tetrahedra that share that spin. Experimentally such axes are formed joining the centres of neighbouring tetrahedra for the A sites of $A_2B_2O_7$ pyrochlore materials because of electrostatic interactions between the orbitals of the magnetic rare earth atoms and non-magnetic oxygen atoms. In this study of hyperkagome spin ice as a $1/4$-doped pyrochlore spin ice I assume a local $<111>$ axis at each magnetic site identical to that of the pyrochlore lattice.

Harris *et al.* were also able to use Pauling's work to estimate the residual entropy of pyrochlore spin ice (specifically $Ho_2Ti_2O_7$). To do this they first assumed the probabilities of different ground state occurrences to be uncorrelated. Then, because Ising spins only have two allowed directions it can be seen that there are 2^N possible configurations of the lattice with N being the number of spins. Of the 16 different possible configurations of spins around a tetrahedron only 6 of them satisfy the two-in/two-out rule of spin ice. This causes a reduction in the degeneracy of the ground state by a factor of $\left(\frac{6}{16}\right)^{N_\triangle}$ where $N_\triangle$ is the number of tetrahedra in the lattice ($\frac{N}{2}$). This leaves a ground state degeneracy of $2^N\left(\frac{6}{16}\right)^{N_\triangle}$. Since $S = k_B \ln\Omega$ with $k_B = 1$ in our unit system and Ω being the degeneracy you get a residual entropy per spin for pyrochlore of $\frac{S}{N} = \frac{1}{2}\ln\frac{3}{2}$. This work was later extended to include corner-shared triangle based lattices by Wills *et al.*(10) who studied the kagome lattice. In their extension instead of spin ice being a two-in/two-out state it became either two-in/one-out or one-in/two-out.

Geometric frustration arises in spin systems on tetrahedral and triangular lattices when symmetries of the lattice make it impossible to simultaneously minimize the energies of each of the interactions between all spins. It is entitled frustration because the lattice has many configurations to choose from to minimize its energy. In a local $<111>$ Ising model the frustration arises when there is a FM interaction between spins. If the easy axes join the centres of neighbouring tetrahedra in a corner-shared tetrahedral lattice, this will cause the optimal case to consist of two

spins pointing towards the centre of a tetrahedron and two away from it, which can be realized in 6 unique but energetically equivalent ways per tetrahedron. For corner-shared triangle lattices with an easy axis pointing either toward the centre of the triangle (kagome(11)) or towards the centre of the doped tetrahedron (kagome, hyperkagome) the equivalent states contain two spins in and one out or vice-versa. There are also 6 unique, energetically equivalent ways of accomplishing this per triangle.

Frustrated Lattices

There are many lattice structures found both in nature and in theoretical studies that exhibit geometric frustration. The most commonly discussed frustrated lattices are the pyrochlore (Fig. 3a) and kagome (Fig. 3c and Fig. 3d right) lattices. A small selection of other lattices include staircase kagome (a pseudo-3D version of the kagome lattice), trillium (3 corner-shared triangles meet at each point), garnet, and hyperkagome (Fig. 3b and Fig. 3d left).

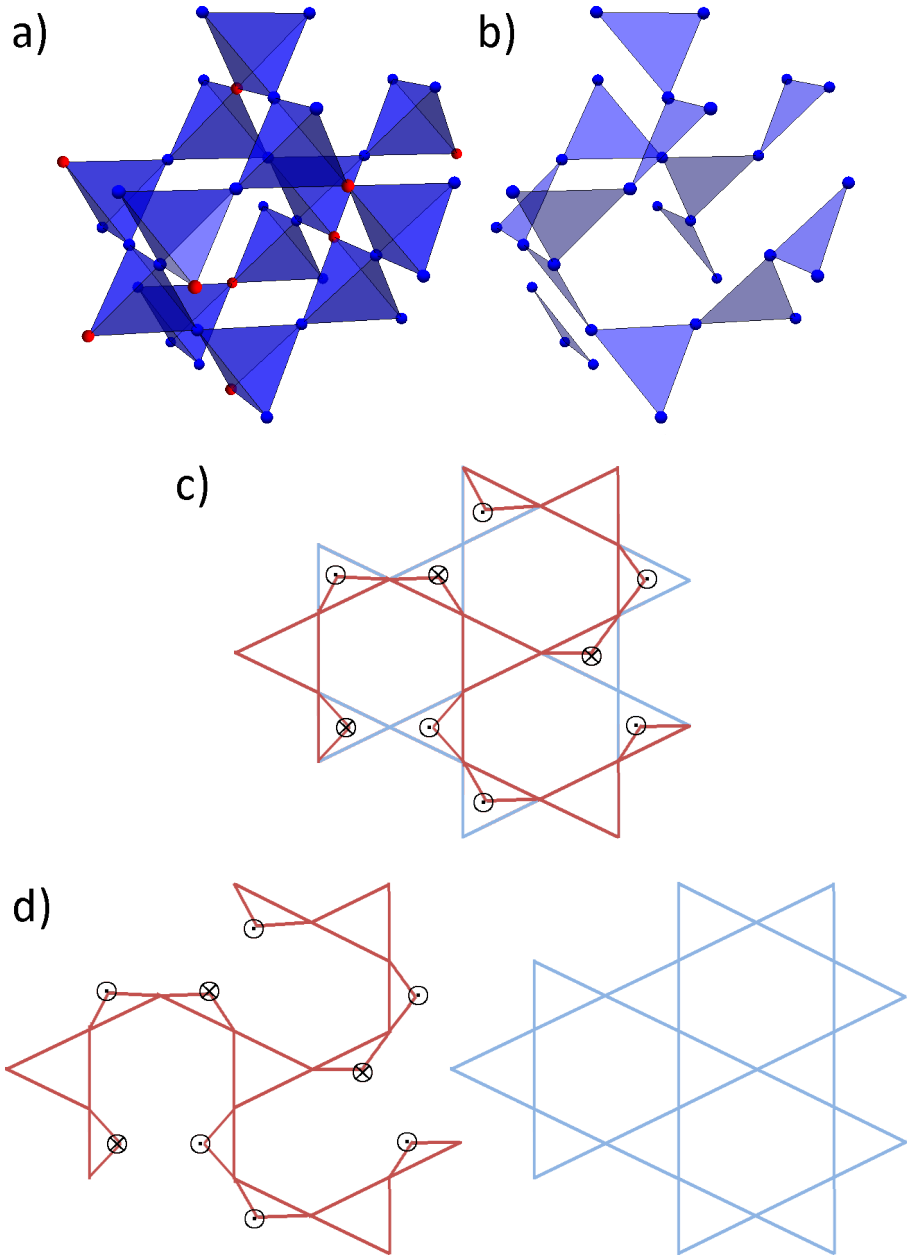

Figure 3: a) The pyrochlore lattice with the sites that need to be doped to obtain the hyperkagome lattice shown in red. b) The same image as in a) but with the doped sites removed to only display hyperkagome. c) Hyperkagome (red) layed overtop of kagome (blue). The spins in the hyperkagome lattice that are above the kagome plane are indicated by a $\odot$ while the spins below the plane are indicated by a $\otimes$. d) The same images as in c) but with the hyperkagome lattice beside the kagome lattice instead of overtop.

The Pyrochlore Lattice

The pyrochlore lattice is a corner-shared tetrahedral lattice (see Fig. 3a). Spin ice on the pyrochlore lattice has been extensively studied both experimentally(8, 12, 13, 14, 15) and theoretically(16, 17, 18, 19, 20) and is one of the most well understood cases of geometric frustration. On the pyrochlore lattice the local $<111>$ directions point between the centres of the two tetrahedra that each spin belongs to. Using the Pauling approximation the ground state entropy per spin expected from spin ice on the pyrochlore lattice following the Bernal-Fowler ice rules(2) is $\frac{S}{N} = \frac{1}{2}\ln(\frac{3}{2})$.

Doping the Pyrochlore Lattice

Ke *et al.*(21) made an important first step towards the realization of hyperkagome spin ice by showing that it was possible to non-magnetically dope the magnetic site of pyrochlore spin ice, and that by doing so one obtained a non-monotonic entropy loss with doping. To explain their results they assumed a completely random doping of the lattice. Their work used the chemical formula $Dy_{2-x}Y_xTi_2O_7$ with non-magnetic yttrium doping the magnetic dysprosium atoms. They then computed the entropy lost to low temperature. This uses the fact that there are only two possible states that each spin can take at high temperature to give the high temperature entropy of $\ln 2$ per Dy spin. The residual entropy is then subtracted from this value. For the pyrochlore lattice with a residual entropy found using the Pauling approximation this results in an entropy loss of $\frac{S_{meas}}{R} = \ln 2 - \frac{1}{2}\ln\left(\frac{3}{2}\right) = \frac{1}{2}\ln\left(\frac{8}{3}\right)$. To calculate the entropy lost they used:

$$\begin{aligned} \frac{S_{meas}(x)}{R} &= \ln 2 - \frac{\ln W(\frac{x}{2})}{N(1-\frac{x}{2})}, \\ W\left(\frac{x}{2}\right) &= 2^{N(1-x/2)} \prod_{i-1}^{4} f_i^{n_i(x/2)}, \\ n_i\left(\frac{x}{2}\right) &= \frac{N}{2} C_4^i \left(1-\frac{x}{2}\right)^i \left(\frac{x}{2}\right)^{4-i}, \end{aligned} \tag{1}$$

where $x/2$ is the nonmagnetic dilution ratio, N is the total number of sites in the lattice, R is the gas constant, C_4^i is the binomial coefficient defined as $C_4^i = \frac{i!}{4!\,(i-4)!}$, and n_i is the number of tetrahedra

with i magnetic sites remaining. The last term, f_i, denotes the fraction of the configurations possible around a tetrahedron with i magnetic sites that satisfy the ground state condition. At $i = 4$ there are 16 possible configurations (2^4) but only 6 of them satisfy the spin ice rules so $f_4 = \frac{6}{16} = \frac{3}{8}$. Similarly, $f_3 = \frac{3}{4}$, $f_2 = \frac{1}{2}$, and $f_1 = 1$. These equations result in the solid line in Fig. 4.

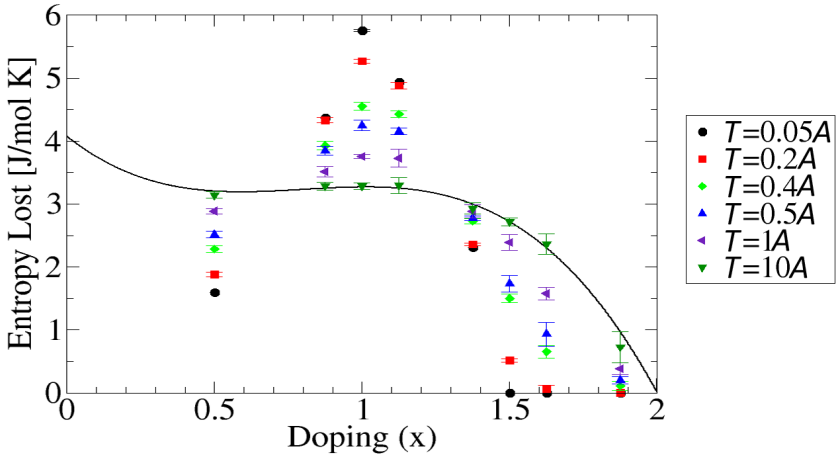

Figure 4: The experimental results of Ke *et al.* are consistent with the solid line, which corresponds to completely random assignments of non-magnetic impurities or the system's sites freezing at temperatures of order 10 times the repulsion between non-magnetic nearest neighbour impurities. The points show the temperature evolution of the entropy lost at different dopings from Monte Carlo studies where the non-magnetic impurities do not freeze but instead are allowed to continue to move to much lower temperature.

For the case of $x = \frac{1}{2}$ (which is where kagome, hyperkagome, and kagome staircase lie) the entropy lost in these units is $R\left(\ln 2 - \frac{1}{3}\ln\left(\frac{9}{2}\right)\right) \approx 1.59 \frac{\text{J}}{\text{mol K}}$. In contrast, the assumption of random site doping inherent to Eq. 1 used by Ke *et al.* and consistent with their data at Yttrium dopings of $\{0.4,\ 1.4,\ 1.8\}$ predicts a much higher loss of entropy at $x = 1/2$, $S_{lost} = 3.203 \frac{\text{J}}{\text{mol K}}$. While the data of Ke *et al.* seems consistent with such a randomly disordered non-magnetic impurity distribution, they have not yet created a $1/4$ doped lattice. In $Dy_{2-x}Y_xTi_2O_7$ the crystal radii(22) as a ratio of the ionic radius of O^{2-} (126pm) of Dy^{3+} (1.052) and Y^{3+} (1.04) are very similar to one another but in the hyperkagome $Na_4Ir_3O_8$ lattice the non-magnetic Na^+ has a much larger

crystal radius (1.16) than that of the magnetic Ir^{4+} (0.765). This raises the question of whether or not size differences between magnetic and their non-magnetic substituent atoms might lead to a net repulsion between non-magnetic sites allowing one to possibly form a more ordered magnetic lattice in a well-controlled synthesis. Frequency of disorder may still make this process difficult to do experimentally. In this sense, the kagome, kagome staircase, and hyperkagome lattices would represent disorder-free $1/4$ dopings of the pyrochlore lattice.

The Kagome Lattice

The kagome lattice can be viewed as a site-ordered limit of a $1/4$ dilution of the pyrochlore lattice in which all the doped atoms happen to lie within specific planes. This lattice has independent planes of connected corner-shared equilateral triangles surrounding hexagons (see Fig. 3c). Despite being a limiting case of magnetically doping the pyrochlore lattice, in theoretical studies to date (11) the direction of the local axes have been taken to point between the centres of the two triangles that each spin belongs to in a 2D analog of pyrochlore spin ice. Wills *et al.*(10) extended the Pauling approximation for the ground state entropy per spin to find that a local FM Ising model on the kagome lattice would result in a larger residual entropy per spin than on the pyrochlore lattice of $\frac{S}{N} = \frac{1}{3}\ln(\frac{9}{2})$.

The Hyperkagome Lattice

As was the case with the kagome lattice, the hyperkagome lattice is also a corner-shared equilateral triangle based, site-ordered limit of a $1/4$ dilution of the pyrochlore lattice. Unlike kagome's planar doping the hyperkagome lattice is fully three dimensional (see Fig. 3b and Fig. 3d). The similarity in dilution with kagome means that hyperkagome has the same increased Pauling approximation for the ground state entropy per magnetic atom spin over that of pyrochlore of $\frac{S}{N} = \frac{1}{3}\ln(\frac{9}{2})$. In this study the local $<111>$ axes have been chosen to be defined for hyperkagome as identical to those of the pyrochlore lattice, pointing between the centres of the tetrahedra each of which features one non-magnetic atom. When comparing the hyperkagome and kagome lattices it can be seen that the

shortest non-repeating loops of the hyperkagome lattice beyond triangles nearly follow the planar hexagons that kagome displays (see Fig. 3c). Each of the hexagons that existed in kagome now has one broken corner. The two separate triangles now lie on different sides of the plane, with one out of the plane atom belonging to a formerly downward-pointing tetrahedron, and the other an upward-pointing tetrahedron. The shortest non-trivial loop in the hyperkagome lattice is 10 sites long.

Beyond Traditional Spin Ice Physics

Research into spin ice systems has recently shown that magnetic monopoles exist in spin ice materials(17). Although rare due to their energy cost, violations of the two-in, two-out rule occur at finite temperature. One of the simplest possible defects arises from flipping one spin in a defect free system. One of the tetrahedra that the spin belongs to now has three spins pointing in and one pointing out while the other has the opposite. This makes the centre of each tetrahedron have a net magnetic moment, one positive and one negative. If the two net magnetic moments are moved sufficiently far away from each other through subsequent spin flips they can both be thought of as magnetic monopoles. Such excitations have been shown to exist on the pyrochlore lattice in $Dy_2Ti_2O_7$(23) and passed some of the tests for the detection of magnetic monopoles(24). Other novel methods of obtaining a pure kagome lattice include the creation of "artificial" spin ices by using electron beam lithography to etch the structure(25) and creating macroscopic spin ice using classical magnets(26).

In this work local $<111>$ Ising spins are restricted to take one of two orientation along local easy axes. Another way, named an Ising model, restricts each spin to take one of two values at each site. What may be the most intuitive ways are known as the antiferromagnetic classical and quantum Heisenberg model within which the spins orient themselves in the most energetically advantageous direction in 3D space.

The speed at which the spins in a spin ice material change direction decreases as the temperature is decreased. Eventually the energy barrier between different ice-rule states will be too high

for thermal fluctuations to access them and the system will freeze into its current state. In low spin systems quantum effects in the material can allow spins to collectively tunnel through these barriers instead of having to find enough energy to go over them. This allows the spin directions to continue to change all the way to 0 temperature. Such systems are known as quantum spin liquids and were first proposed by Anderson in 1973(3). The search for the existence of quantum spin liquids is currently a major research effort in this field. The frustrated lattice $Na_4Ir_3O_8$ which forms on the hyperkagome lattice is one candidate for a quantum spin liquid(27).

Although it has recently become easier to find good realizations of kagome spin systems they have been historically difficult to find. This may be due to materials being inherently three-dimensional. After decades of searching the first experimental realization of antiferromagnetic correlations on a structurally perfect spin $1/2$ kagome lattice appeared in $ZnCu_3(OH)_6Cl_2$ in 2005(28, 29). Even in these materials questions remain about whether they are realizations of a purely kagome lattice, given that non-magnetic site disorder may be of the order of 6% in the Cu plane(30).

In This Thesis

This thesis investigates the properties of a local $<111>$ Ising model on the hyperkagome lattice with an interaction beyond the simple nearest neighbour interaction. With just a nearest neighbour interaction frustration arises on the hyperkagome lattice given a ferromagnetic nearest neighbour interaction. This interaction causes the lattice to enter a two in/(out), one out/(in) spin ice state. The nearest neighbour interaction no longer needs to be ferromagnetic in order for a spin ice state to arise when a dipole-dipole interaction is added, instead only the effective nearest neighbour interaction needs to be ferromagnetic. Therefore, as has been seen on the pyrochlore lattice(18), as long as the dipole-dipole interaction strength is sufficiently large in comparison to the nearest neighbour interaction strength a spin ice state will occur even with an antiferromagnetic nearest neighbour interaction. After a spin ice state has been reached two further transitions arise purely from the dipole-dipole interaction and are comparable to the states found(11) on the kagome lattice with a

dipole-dipole interaction. This places the hyperkagome lattice at an interesting crossroad between the two-dimensional, triangular based kagome lattice and the three-dimensional, tetrahedron based pyrochlore lattice.

The following three chapters will describe the model used to simulate the interactions on the hyperkagome lattice, discuss the results of those simulations, and conclude with a discussion of possible extensions to the work done here. The description of the model will include a description of the dipole-dipole interation and effective nearest neighbour interaction between the magnetic atoms int he hyperkagome lattice as well as the Monte Carlo method and loop algorithm used to run the numerical simulations. The discussion of the results starts with results of numerically doping the pyrochlore lattice before moving through the steps towards a full simulation of the hyperkagome lattice with dipole-dipole interactions and the loop algorithm. The discussion will then describe the outcome of the simulations and compare it to both the pyrochlore and garnet lattices before finishing with a discussion of the residual entropy. The final chapter will summarize the work as well as discuss a possible extension to the numerical doping of the pyrochlore lattice.

α	$\hat{e}^{\alpha}$
a	$\frac{1}{\sqrt{3}}(1,1,1)$
b	$\frac{1}{\sqrt{3}}(-1,1,-1)$
c	$\frac{1}{\sqrt{3}}(-1,-1,1)$
d	$\frac{1}{\sqrt{3}}(1,-1,-1)$

Table I: The 12 inequivalent sites of Table II (labeled a_1 through d_3) have only 4 inequivalent $<111>$ axes labeled a through d. These easy axes are denoted by unit vectors labeled $\hat{e}^{\alpha}$.

Chapter II: Model

This work studied in this thesis is a local $<111>$ Ising model on the hyperkagome lattice. Each spin can then be written as $\vec{s}_i^{\alpha} = \sigma_i^{\alpha}\hat{e}^{\alpha}$ where $\sigma_i^{\alpha} = \pm 1$ and $\hat{e}^{\alpha}$ is a unit vector denoting the local easy axis as presented in Table I. This work studies an antiferromagnetic interaction between neighbouring spin vectors using the nearest neighbour Hamiltonian:

$$\mathscr{H}_{NN} = J \sum_{<(i,\alpha),(j,\beta)>} \vec{s}_i^{\alpha} \cdot \vec{s}_j^{\beta}, \tag{2}$$

where J is used to moderate the strength of the nearest neighbour interaction and $<(i,\alpha),(j,\beta)>$ is a sum over nearest neighbour spins. A value of $J > 0$ produces the required antiferromagnetic interaction.

The hyperkagome lattice has 12 spins within its cubic unit cell. The relative location of each spin within its unit cell is shown in Table II with α giving an alphabetic designation to a site, and k a number between one and four. The four apparently missing indices: $\{a_2,\ b_3,\ c_1,\ d_4\}$ correspond to spins in the pyrochlore lattice that have been doped with non-magnetic atoms. The smallest, non-trivial loop in the lattice is 3D and encompasses 10 spins. The loops form from two intersecting planar half loops of 6 spins each (with 2 overlapping).

Dipole-dipole Interaction

The dipole-dipole interaction comes from treating the atomic spins as tiny dipoles with a positive magnetic charge on one end and a negative magnetic charge on the other. The dipole-dipole in-

α	x	y	z
a_1	0	0	0
a_3	0	1/2	1/2
a_4	1/2	0	1/2
b_1	0	3/4	3/4
b_2	1/2	1/4	3/4
b_4	1/2	3/4	1/4
c_2	1/4	1/2	3/4
c_3	3/4	1/2	1/4
c_4	1/4	0	1/4
d_1	3/4	3/4	0
d_2	1/4	1/4	0
d_3	3/4	1/4	1/2

Table II: The relative location of each spin within the 12 site unit cell of the hyperkagome lattice.

teraction is an action at a distance meaning that it is between more than just nearest neighbour spins. In fact, the dipole-dipole interaction is an infinite range interaction so all spins in a material will interact with all others and that the dipole-dipole Hamiltonian ($\mathscr{H}_{DD}$) contains an infinite summation. The dipole-dipole Hamiltonian has the form

$$\mathscr{H}_{DD} = Dr_{NN}^3 \sum_{\substack{i>j \\ \alpha,\beta}} \left(\frac{\vec{s}_i^{\alpha} \cdot \vec{s}_j^{\beta}}{|\vec{r}_{ij}^{\alpha\beta}|^3} - \frac{3(\vec{s}_i^{\alpha} \cdot \vec{r}_{ij}^{\alpha\beta})(\vec{s}_j^{\beta} \cdot \vec{r}_{ij}^{\alpha\beta})}{|\vec{r}_{ij}^{\alpha\beta}|^5} \right), \tag{3}$$

where r_{NN} is the distance between nearest neighbour spins and $\vec{r}_{ij}^{\alpha\beta}$ is a vector that points from spin $\vec{s}_i^{\alpha}$ to spin $\vec{s}_j^{\beta}$. When done in 2D systems this infinite summation is handled by truncating after a set distance(31) but this has been shown to be insufficient in 3D systems such as pyrochlore(18). Instead, Ewald summation has been used to change the summation to one that is bound by the size of the simulation(32). Ewald summation casts the summation in real space to two rapidly converging summations, one in real and one in phase space. Code to calculate the value of the D_{ij} terms for hyperkagome was developed prior to the start of this work(33).

The total Hamiltonian ($\mathscr{H}$) is the sum of the nearest neighbour and dipolar Hamiltonians which, after Ewald summation, is

$$\mathscr{H} = J \sum_{<(i,\alpha),(j,\beta)>} \vec{s}_i^{\alpha} \cdot \vec{s}_j^{\beta} + Dr_{NN}^3 \sum_{\substack{i>j \\ \alpha,\beta}} D_{ij} \sigma_i^{\alpha} \sigma_j^{\beta}, \tag{4}$$

where the D_{ij} terms come from a strictly upper diagonal matrix of interaction terms between neighbours of differing distances as calculated by the Ewald summation as shown in Appendix A. The summation over $i > j$ is now bounded to be within the periodic boundaries of the system instead of infinite.

Effective Nearest Neighbour Interaction Strength

In order to scale the energies of trials with different nearest neighbour and dipolar interaction strengths so that they are comparable it is useful to define an effective nearest neighbour interaction strength. This interaction strength is computed by only considering the nearest neighbour terms in the Hamiltonian. When only a single nearest neighbour term is considered in Eq. 2, $\mathscr{H}_{NN} = J(\hat{e}^{\alpha} \cdot \hat{e}^{\beta}) \sigma_i^{\alpha} \sigma_j^{\beta}$. The dot product between any two of the $<111>$ Ising vectors results in $\hat{e}^{\alpha} \cdot \hat{e}^{\beta} = -\frac{1}{3}$. This gives a nearest neighbour portion to this effective interaction of $J_{NN} = -\frac{J}{3}$. The dipolar term in the Hamiltonian has a nearest neighbour distance ($\vec{r}_{ij}^{\alpha\beta}$) defined to be 1. For the first term in the summation in Eq. 3 the nearest neighbour spin dot product remains $-\frac{1}{3}\sigma_i^{\alpha}\sigma_j^{\beta}$ as it was in the nearest neighbour portion of the effective interaction. The second part of the summation results in $(\vec{s}_i^{\alpha} \cdot \vec{r}_{ij}^{\alpha\beta})(\vec{s}_j^{\beta} \cdot \vec{r}_{ij}^{\alpha\beta}) = -\frac{2}{3}\sigma_i^{\alpha}\sigma_j^{\beta} \left|\vec{r}_{ij}^{\alpha\beta}\right|^2$ which is the same for all lattices whose spins are directed towards the centres of the pyrochlore lattices tetrahedra(19). Combining the two parts of the summation you get an effective nearest neighbour dipolar term of $D_{NN} = D\left(-\frac{1}{3} - 3\left(-\frac{2}{3}\right)\right) = \frac{5D}{3}$. When combined into the total effective interaction strength one gets $J_{eff} = J_{NN} + D_{NN} = -\frac{J}{3} + \frac{5D}{3}$ identical to that of the pyrochlore lattice. For comparison, the effective nearest neighbour interaction strength on kagome whose local axes point between the centres of neighbouring triangles within a 2D plane is $J_{eff} = -\frac{J}{2} + \frac{7D}{2}$(11).

The effective nearest neighbour interaction strength can be used as

$$\mathscr{H} = J_{eff} \sum_{<ij>} \sigma_i \sigma_j + [\text{Higher Order Terms}] \tag{5}$$

where the higher order terms arise from interactions with further neighbours and i and j implicitly carry the information of the previous letters and number α_i. A simple rearranging of the effective strength gives $J_{eff} = J_{NN} + D_{NN} = \left(\frac{J_{NN}}{D_{NN}} + 1\right) D_{NN}$ which shows that if the higher order terms are 0 there would be no coupling between spins for a value of $J_{NN}/D_{NN} = -1$. This has been shown to not be the case on the pyrochlore lattice(19) where the coupling was found to go to zero at $J_{NN}/D_{NN} \approx -0.91$. It will be shown below that the higher order terms are also non-zero for the hyperkagome lattice and that at least for the $L = 1$ case, and within error for larger L, the critical ratio of J_{NN}/D_{NN} is the same as found on the pyrochlore lattice.

Monte Carlo

The Monte Carlo used for this work was derived from the simulated annealing prescription of Kirkpatrick *et al.*(34). Simulated annealing is a method that allows for a good approximation of the optimum solution to a problem when analytical solutions become impractical given the large number of objects (in this case spins). It does this through the use of the Metropolis algorithm(35) and through the slow reduction of the simulated temperature reducing the number of states accessible to the simulation. To use this algorithm the lattice needs to be initialized by assigning the spins random directions. The simulated temperature was set to a sufficiently high value to allow complete equilibration of the lattice before beginning to map out regions where some of phase space becomes restricted due to the Monte Carlo condition. A random spin or set of spins is then chosen to attempt to update and the difference in energy (δE) if these spins were to be changed is computed. If the energy has been reduced or remains constant then the updates are always accepted, the Metropolis algorithm comes in when the energy of the system is increased. In this case a random number between zero and one inclusive is chosen. If this random number is less than $e^{-\frac{\delta E}{T}}$ then the update is accepted. When T is large this exponential is almost always 1 meaning

that all updates are accepted. As T is slowly reduced energy differences will need to be smaller for a proposed update to have a significant chance of being accepted. In this work T is reduced by 1% at each step. This allows the simulation to sample fewer temperatures at high temperature where the lattice is still in a paramagnetic state but still sample enough temperatures at lower temperature to allow for proper equilibration in areas of restricted phase space and increase the resolution of the transition peaks.

At each temperature a certain number of Monte Carlo steps are carried out. A Monte Carlo step is enough random spin updates that on average one update per spin is attempted. Most of the Monte Carlo steps are done to equilibrate the lattice at its new temperature and no information is gained from them but the steps following this are run to allow for averaging of thermodynamic quantities (typically energy and heat capacity) over the accessed phase space.

Lattices are defined spatially by the smallest set of unique spin locations (sites) that can fully describe the lattice. The box that bounds these spins is called the unit cell. If you move the unit cell by an integer number of units along any of the x, y, or z axes the relative positions of the spins that lie within the box will not have changed. The size of the lattice simulated is often described using the number of unit cells present. For this work the simulation will always be cubic with L unit cells along each of the x, y, and z directions. This means there will be L^3 unit cells in the simulation with the largest value of L simulated here being 4, the same maximum size as studied by Melko *et al.* for the dipolar spin ice model on the pyrochlore lattice(18). Periodic boundary conditions are used to handle the outside surfaces of the simulated lattice. If the nearest neighbour of a spin lies outside of the defined unit cells the equivalent spin on the opposite side of the lattice is used. This allows us to study an area of space that is effectively contained within a larger lattice.

The Loop Algorithm

The simplest algorithm for updating the spins when running Monte Carlo is known as the single spin flip algorithm. With single spin flip you simply take a random spin within the lattice and you flip it (change the sign of σ_i^α) if it meets the Monte Carlo criteria. As was seen in both the kagome

and pyrochlore dipolar spin ice model studies(11, 19) ergodicity was lost at low temperatures when only using a single spin flip algorithm. In order to remain ergodic to lower temperatures a loop algorithm was implemented.

The loop algorithm is comparable to a constrained random walk. A random starting location is chosen then it attempts to find a path through the lattice. The constraint is the same as the one used on the pyrochlore lattice(19) which is itself modified from an algorithm developed by Berkema and Newman(36) for square ice models. The constraint requires that the loop moves from a spin directed into a triangle to one directed out of the triangle. This means that the loop will alternate between positive and negative values of σ. This also means that the lattice must be in a spin ice state for the loop algorithm to work. There are two different loop algorithms that differ in how they determine when the loop is considered complete (see figure 5). The long loop algorithm requires the starting spin to be found again before the loop is complete while the short loop algorithm only requires that any spin already in the loop be found and the "tail" that goes from the starting spin to that spin be excluded from the loop. For this work a short loop algorithm was implemented. In the case that the algorithm attempts to find a loop but instead comes to a point where it is not possible to continue due to the constraints on the random walk, a single spin flip is attempted on a random site instead.

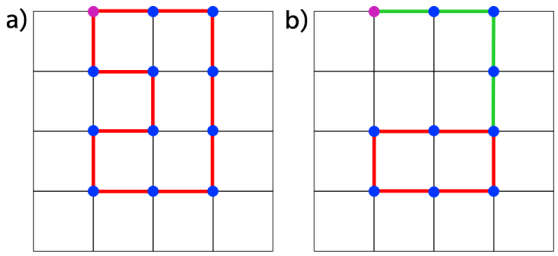

Figure 5: a) In the long loop algorithm the last site in the loop must also be the first site. This means that all sites visited will be used as part of the loop. b) In the short loop algorithm once a site is visited that has already been visited a loop has been formed. The "tail" section that goes from the first spin to that spin (the green lines) is discarded.

Above the spin ice crossover the loop algorithm is not only not needed as ergodicity is maintained with only a single spin flip algorithm but its inclusion actually causes incorrect physics to be

displayed as it favours loop moves. Due to the restriction in the random walk the lattice will prefer to be in a spin ice state. This causes a depression in the peak of the heat capacity representing the spin ice crossover. Because of this behaviour the loop algorithm was only enabled after the lattice had established itself in the spin ice state as determined from a calculation of the average of the nearest neighbour component of the Hamiltonian (see Eq. 2) over all Monte Carlo steps at the current temperature. This value is constant below the spin ice crossover. While this is a known issue with loop algorithms on the pyrochlore lattice(37) it does not appear to have been mentioned in the literature. When the loop algorithm is enabled single spin updates are still carried out, at each step either the loop update or a single spin update is done at random.

In the fastest case to test ($L = 1$) a simple loop algorithm did not help to restore ergodicity at low temperature. Looking at the ground states that exist at $L = 1$ it was determined that two independent loops would be needed in order to move from one ground state to another. A double loop algorithm was implemented and the heat capacity from the Monte Carlo simulations was found to match an analytical treatment we developed at $L = 1$, as will be described below (see also Fig. 6a).

The increased runtime caused by the double loop algorithm reduced how large L could be and still have the simulations run in reasonable time. The comparison between the single and double loop algorithm was done at $L = 2$ to determine if the double loop algorithm was still needed in a non-trivial case and it was found that there was no longer a difference in the heat capacities found by the two methods (see Fig. 6b). This was used as justification to only use the single loop algorithm when simulating larger values of L. Looking at the heat capacity for $L = 4$ (see Fig. 6c) both low temperature transition peaks are obtained with just the single loop algorithm. Unlike the case at $L = 1$ the system no longer maintains a non-zero acceptance rate to $T = 0$, suggesting that ergodicity of our single loop algorithm may be lost as the system enters its almost fully ordered ground state. Both the single spin flip and single loop acceptance rate (percentage of times an update meets the Monte Carlo criteria) goes to 0 after the transitions. In order to be comparable with the per spin statistics of the single spin flip acceptance rate the loop acceptance rate is shown

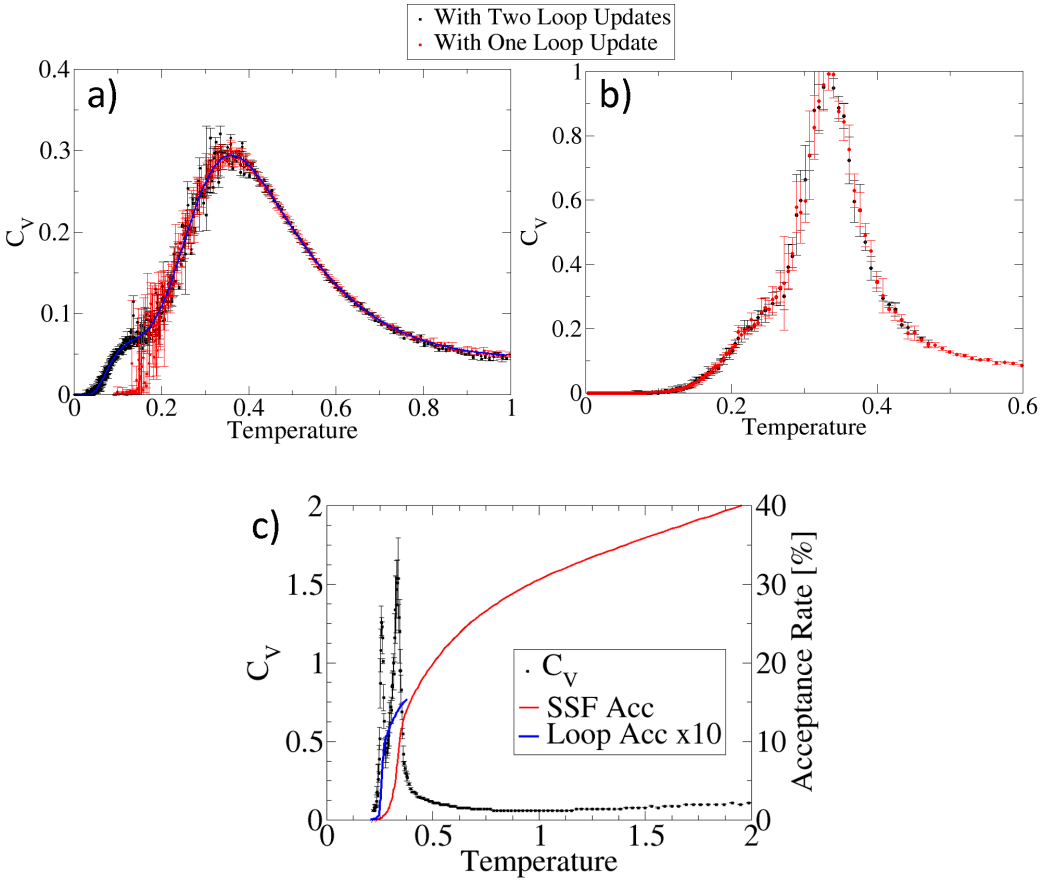

Figure 6: a) The heat capacity when using both a single (red) and double (black) loop algorithm at L=1. The double loop algorithm is always within error of the analytical result (blue) but at low temperature the single loop algorithm is not. b) The heat capacity when using both a single (red) and double (black) loop algorithm at L=2. c) At $L = 4$ the acceptance rate of the single spin flip algorithm goes to zero at the peak of the spin ordering transition but the single loop acceptance rate remains non-zero until after this transition. All heat capacities are for $J_{NN}/D_{NN} = -\frac{1}{5}$.

as 10 times the percentage of loops accepted as the smallest possible loop in the lattice follows 10 sites. One sees that the loop algorithm is the dominant spin flipping process through both of the ordering transitions which will be described below.

In future work it may be possible to introduce "loop" updates which satisfy the ground state spin constraints while not forming closed loops. Such updates are possible on triangle-based lattices, but not possible on tetrahedron-based lattices like pyrochlore spin ice.

Chapter III: Results

Numerically Doping the Pyrochlore Lattice

Since our study of hyperkagome spin ice was quite motivated by the possibility of non-magnetically doping pyrochlore spin ice, it is interesting to consider simple models which might lead to a more ordered magnetic lattice, and the effect this site order would have on the entropy lost as a function of non-magnetic doping. To address this question, temperature dependent Monte Carlo was run with a repulsion term between nearest neighbour doped sites. The Hamiltonian used in the Monte Carlo is shown in Eq. 6. In it A is the repulsion strength, $\langle ij \rangle$ is a sum over nearest neighbour sites, and η is 1 on doped sites and 0 on non-doped sites.

$$\mathscr{H} = A \sum_{\langle ij \rangle} \eta_i \eta_j. \tag{6}$$

Eq. 1 was then used, with a modification of n_i to compute the entropy lost at several temperatures. Replacing n_i was a count of the number of tetrahedra with each number of magnetic atoms remaining on them calculated from the Monte Carlo's output of the location of the doped sites. The temperature evolution (in units of the repulsion between the non-magnetic impurities) of the entropy loss is shown in Fig. 4. Within this approximation the entropy lost for a $\frac{1}{4}$ doping is now in agreement with the Pauling estimate. One might expect that the non-magnetic and magnetic atoms in a realistic lattice will not be free to move below some temperature. While in $Na_4Ir_3O_8$(38) it has been shown that a $1/4$-Na-doped corner-shared tetrahedral lattice can give rise to a hyperkagome lattice, it is interesting to note that for our simulations the lattice tended to not choose a doped state that corresponded to a previously mentioned lattice configuration. While this material features a corner-shared equilateral triangle magnetic lattice doped with non-magnetic Na sites, it is worthwhile to note that this is not a non-magnetically doped pyrochlore lattice do to the presence of extra sodium atoms. A study of further-neighbour interactions might be useful to determine if it is possible for this process to lead to one of the site specific dopings of the pyrochlore lattice

discussed earlier.

Setup

All Monte Carlo trials that were done used 200000 Monte Carlo steps for equilibrating to ensure that the loop algorithm had a chance to explore all states that it was possible for it to as well as a further 5000 Monte Carlo steps for averaging. Most of the results were obtained using a lattice size of $L = 4$ which contains 768 spins. The major results of the Monte Carlo are derived from the heat capacity, the equation for which can be derived from the canonical ensemble average of classical statistical mechanics:

$$\langle A \rangle = \frac{\int A e^{-\beta \mathscr{H}} d\tau}{\int e^{-\beta \mathscr{H}} d\tau}, \tag{7}$$

where $\langle A \rangle$ is the ensemble average of the value A, $\beta \equiv \frac{1}{k_B T}$ with T being the simulated temperature and k_B being the Boltzmann constant (defined to be 1 in our unit system), $\mathscr{H}$ is the Hamiltonian of the system, and $d\tau$ is the volume element of the phase space of interest. The denominator of Eq. 7 is the partition function (Z) of the ensemble. In the case of the internal energy (U) Eq. 7 is:

$$U = \langle \varepsilon \rangle = \frac{\int \varepsilon e^{-\beta \varepsilon} d\varepsilon}{\int e^{-\beta \varepsilon} d\varepsilon}. \tag{8}$$

Given the definition of heat capacity as $C_V \equiv \left(\frac{\partial U}{\partial T}\right)_V$ the derivative can be distributed through Eq. 8:

$$\begin{aligned} \frac{dU}{dT} &= \frac{\int \varepsilon \frac{de^{-\beta\varepsilon}}{dT} d\varepsilon}{\int e^{-\beta\varepsilon} d\varepsilon} - \frac{\left(\int \varepsilon e^{-\beta\varepsilon} d\varepsilon\right)\left(\int \frac{de^{-\beta\varepsilon}}{dT} d\varepsilon\right)}{\left(\int e^{-\beta\varepsilon} d\varepsilon\right)^2} \\ \frac{dU}{dT} &= \frac{\int \varepsilon^2 e^{-\beta\varepsilon} d\varepsilon}{k_B T^2 \int e^{-\beta\varepsilon} d\varepsilon} - \frac{\left(\int \varepsilon e^{-\beta\varepsilon} d\varepsilon\right)^2}{k_B T^2 \left(\int e^{-\beta\varepsilon}\right)^2}. \end{aligned} \tag{9}$$

Noticing from Eq. 7 that the first term contains the ensemble average of the quantity ε^2 and the second term contains Eq. 8 squared the form of the heat capacity as used while running the Monte

Carlo is:

$$C_V = \frac{\langle \varepsilon^2 \rangle - \langle \varepsilon \rangle^2}{k_B T^2}. \tag{10}$$

From the heat capacity the transition/crossover temperatures can be determined as well as the residual entropy as a function of temperature.

Analytics

At $L = 1$ it is possible to analytically determine the properties of the hyperkagome lattice. This is done by first calculating the partition function

$$Z = \sum_{\text{all states}} e^{-\frac{\varepsilon}{k_B T}} \tag{11}$$

where ε is the energy of that state with the form of the Hamiltonian and the Boltzmann constant (k_B) is still defined to be 1. Since each spin can only be in one of two possible positions the number of states is 2^{12L^3} which at $L = 1$ is 4096 (compared to the roughly 7.9×10^{28} states at $L = 2$). From there the internal energy of the system as well as the heat capacity both as a function of temperature can be found using:

$$\begin{aligned} U &= T^2 \frac{\partial}{\partial T} \ln Z, \\ C_V &= \frac{\partial}{\partial T} U. \end{aligned} \tag{12}$$

When the heat capacity graphs for different values of J_{NN}/D_{NN} are observed two distinct regions can be seen. One region (for $J_{NN}/D_{NN} < -0.91$) has just a single transition to an ordered antiferromagnetic state as seen in Fig. 7a. The other region ($J_{NN}/D_{NN} > -0.91$) has three separate peaks as seen in Fig. 7b. The first peak is a crossover to a spin ice state followed by peaks indicating transitions to a charge ordered and then a state that was not possible to classify for a lattice size this small. For values of $J_{NN}/D_{NN} \approx -0.91$ the antiferromagnetic state and the spin ordered states begin to exist at similar energies resulting in amplified peaks or additional peaks arising.

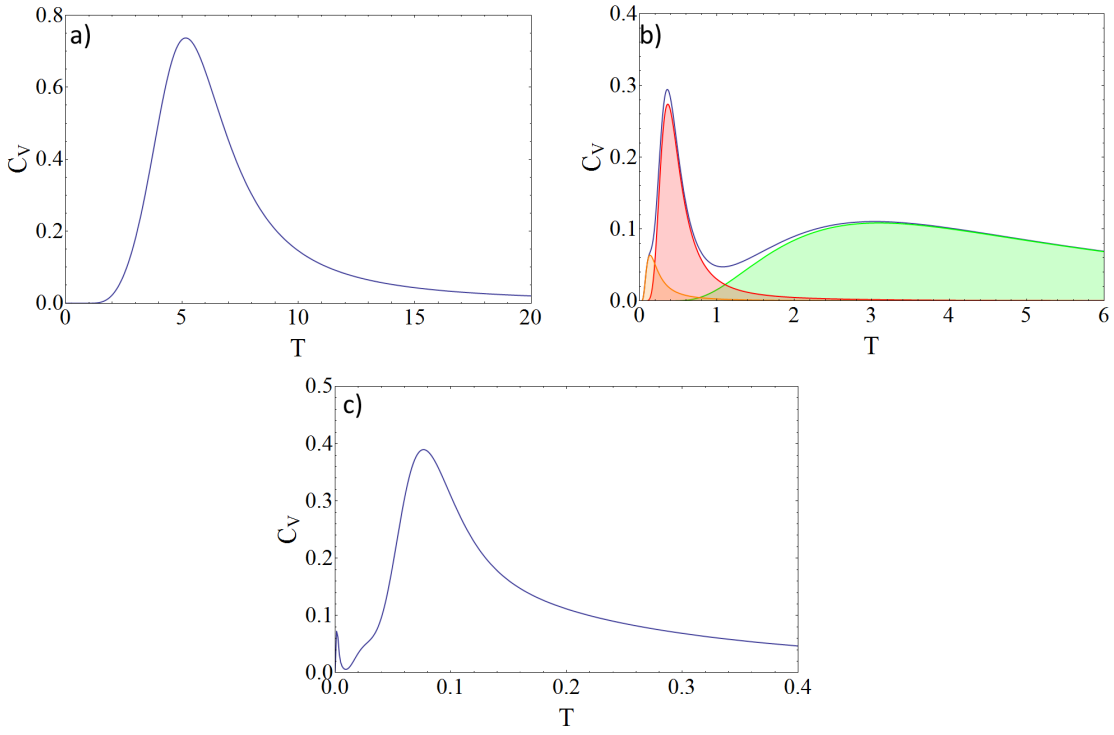

Figure 7: The heat capacities as obtained from analytics for a) $J_{NN}/D_{NN} = -2$, b) $J_{NN}/D_{NN} = -\frac{1}{5}$ and c) $J_{NN}/D_{NN} = -0.905$, just short of the transition at $J_{NN}/D_{NN} \approx -0.91$.

At the point in which the antiferromagnetic state and the spin ordered state exist at the same energy the spins will become decoupled. As was seen on the pyrochlore lattice with a dipole-dipole interaction(19) this occurs at $J_{NN}/D_{NN} \approx -0.91$.

When the states of the lattice are written out (see the ground state and first excited state in Table III) they can be separated into groups that satisfy each of the ground state conditions. This allows for exact determination of the peak location for $J_{NN}/D_{NN} > -0.91$ where this would have given results that were offset because of the overlap of the peaks or have been completely impossible to determine for the spin ordered peak. It also allows a look at what might be expected of the residual entropy at larger values of L by counting the number of states that satisfy the constraints of each region. As it turns out later the only one that is relevant at higher L (see subsection The Long Range Dipole-dipole Interaction) is that of the spin ordered state which has 6 states. This leaves a residual entropy of $\frac{S}{N} = \frac{1}{12}\ln 6 \approx 0.149313$.

State	σ_{a_1}	σ_{b_1}	σ_{d_1}	σ_{b_2}	σ_{c_2}	σ_{d_2}	σ_{a_3}	σ_{c_3}	σ_{d_3}	σ_{a_4}	σ_{b_4}	σ_{c_4}
Ground	-1	1	1	1	-1	1	1	1	-1	1	-1	1
Ground	1	-1	-1	-1	1	-1	-1	-1	1	-1	1	-1
Ground	-1	1	-1	-1	-1	1	-1	1	-1	1	-1	-1
Ground	-1	-1	1	1	-1	-1	1	-1	-1	-1	-1	1
Ground	1	1	-1	-1	1	1	-1	1	1	1	1	-1
Ground	1	-1	1	1	1	-1	1	-1	1	-1	1	1
1^{st}	-1	1	1	1	-1	1	1	-1	1	-1	1	1
1^{st}	1	-1	-1	-1	1	-1	-1	1	-1	1	-1	-1
1^{st}	-1	-1	1	-1	-1	1	1	-1	-1	1	-1	-1
1^{st}	-1	1	-1	-1	-1	1	-1	-1	1	-1	1	-1
1^{st}	-1	1	1	-1	1	1	-1	1	1	1	-1	1
1^{st}	1	-1	-1	1	-1	-1	1	-1	-1	-1	1	-1
1^{st}	1	-1	1	1	1	-1	1	1	-1	1	-1	1
1^{st}	1	1	-1	1	1	-1	-1	1	1	-1	1	1
1^{st}	-1	1	-1	1	-1	-1	-1	1	-1	-1	-1	1
1^{st}	-1	-1	1	-1	1	-1	-1	-1	1	-1	-1	1
1^{st}	1	1	-1	1	-1	1	1	1	-1	1	1	-1
1^{st}	1	-1	1	-1	1	1	1	-1	1	1	1	-1

Table III: The 6 ground states and 12 first excited states of hyperkagome at $L = 1$.

Before the Long Range Dipole-dipole Interaction

The first simulations that were run on the lattice only made use of the nearest neighbour interaction ($D = 0$). A ferromagnetic interaction was simulated that showed a single crossover to a spin ice state as seen previously(39). The next step towards the long range dipole-dipole interaction was to truncate the summation in $\mathscr{H}_{DD}$ at nearest neighbours and make the nearest neighbour interaction antiferromagnetic (as is the case for the experimental pyrochlore spin ice systems studied to date(20)). With just a nearest neighbour dipolar term with a strength $D = 1$ the effective nearest neighbour interaction strength is $J_{eff} = \frac{4}{3}$ as compared to the effective strength in the no dipolar case of $J_{eff} = \frac{1}{3}$. This means that the nearest neighbour dipolar simulation had a stronger FM interaction than the case without dipolar so it should be expected to give the same transition to a spin ice state. As shown in Fig. 8b this is exactly what happened. The nearest neighbour dipolar interaction is also size independent, displaying a crossover at the same temperature and with the same increase in heat capacity for all tested lattice sizes (up to $L = 6$).

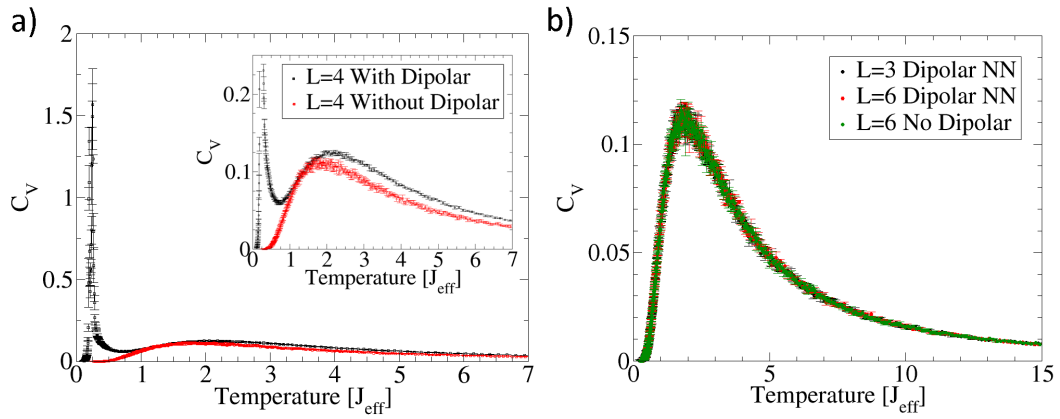

Figure 8: a) Comparison of the heat capacity with a ferromagnetic nearest neighbour interaction ($J = -1$) and no dipolar interaction (in red) with that of a antiferromagnetic nearest neighbour interaction ($J = 1$) and a dipole-dipole interaction ($D = 1$). b) Comparison of the same non-dipolar trial with a trial that had a nearest neighbour dipolar interaction.

The Long Range Dipole-dipole Interaction

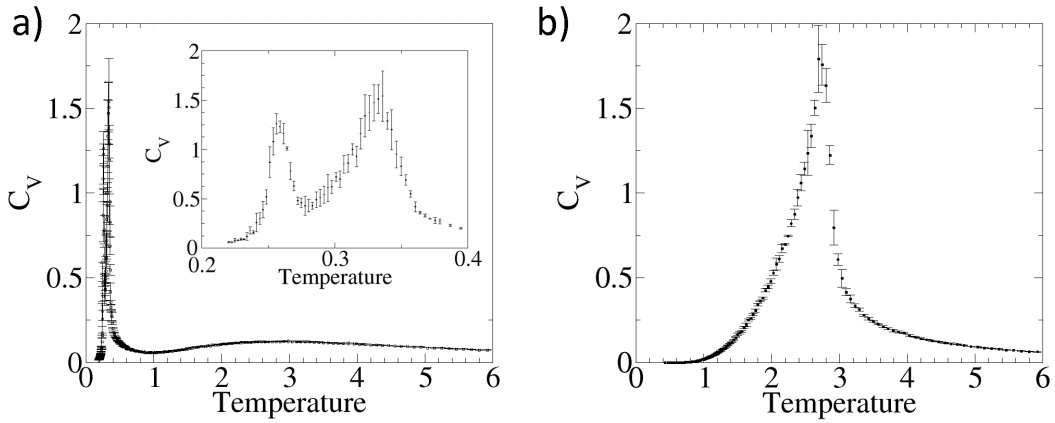

Figure 9: a) The heat capacity at $L = 4$ for $J_{NN}/D_{NN} = -\frac{1}{5}$. Inset is a blow-up of the lower temperature peaks to more clearly show that two peaks are present. b) The heat capacity at $L = 4$ for $J_{NN}/D_{NN} = -2$.

At $L = 4$ the low temperature spin ordering transition becomes much more distinct from the charge order peak than it was at $L = 1$ and 2. The two transition peaks also become much sharper as one would expect from a transition as opposed to a crossover. The data shown in Fig. 9 is averaged from four independent trials of the Monte Carlo with the same values of J and D. They have error bars which are determined from the standard deviation of the four trials:

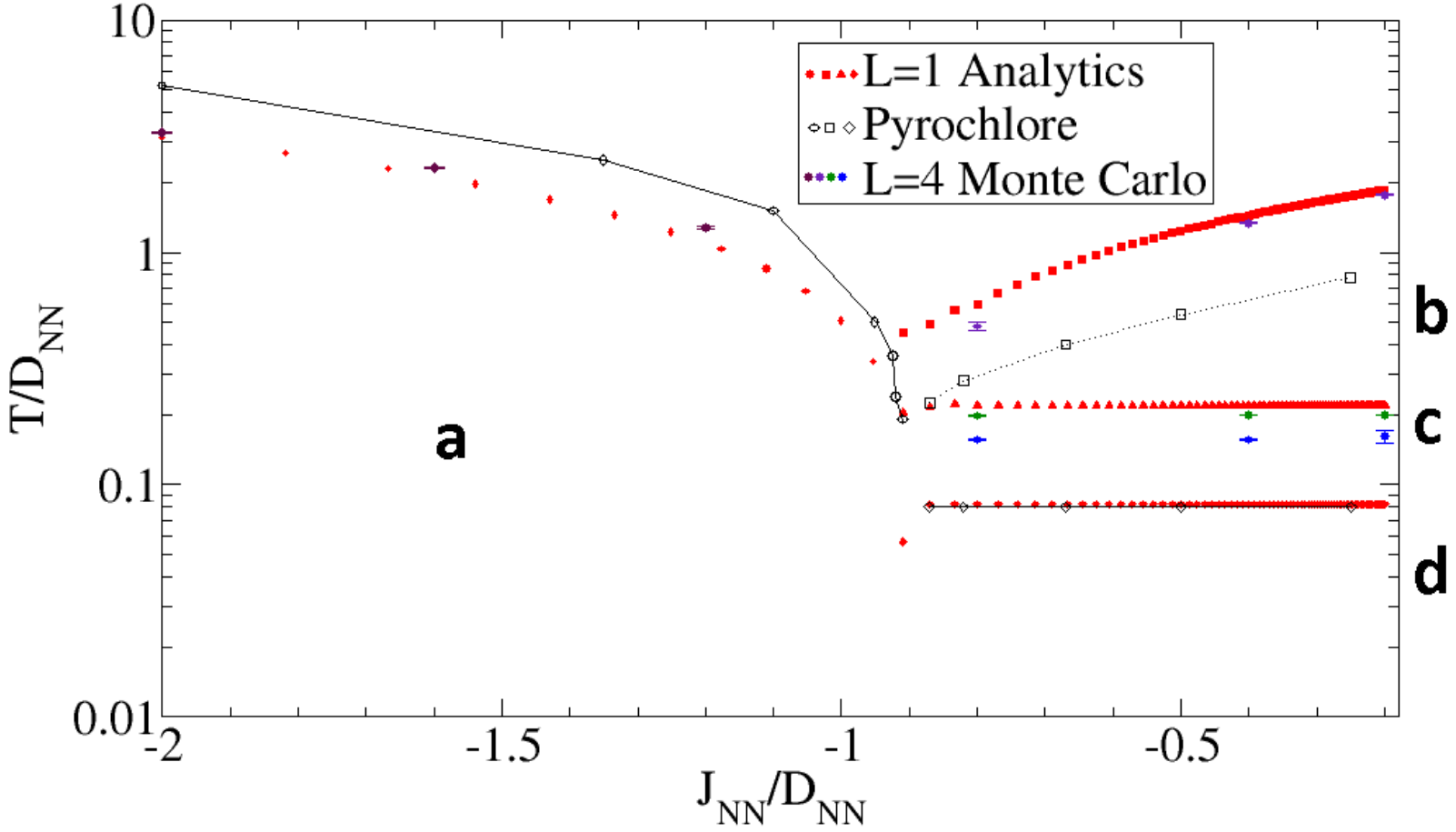

Figure 10: The phase diagram for the hyperkagome and pyrochlore(18) lattices. Both lattices show a transition to an antiferromagnetic state (a) for $J_{NN}/D_{NN} < -0.91$. For $J_{NN}/D_{NN} > -0.91$ hyperkagome displays three peaks in its heat capacity that correspond to: a crossover to a spin ice state (b), a transition to a charge ordered state (c), and a transition to a spin ordered state (d). In this region pyrochlore also shows a crossover to a spin ice state but that is only followed by a single transition to an ordered ground state.

$$\delta C_V(T) = \sqrt{\frac{\sum_{i=0}^{4}\left(C_{V,i}(T) - \bar{C_V}(T)\right)^2}{12}}, \tag{13}$$

with $\bar{C_V}(T)$ being the average heat capacity at the given temperature. The location of the peaks is determined for each trial separately instead of from the averaged heat capacity. This allows the four independent estimates for the peaks of the discrete data to be averaged and provide error bars using Eq. 13 but with peak location instead of heat capacity.

Similar to what was seen in pyrochlore the spin ice state continues to exist even with an antiferromagnetic nearest neighbour exchange down to $J_{NN}/D_{NN} \approx -0.91$. Below this only a single transition is seen to an ordered antiferromagnetic ground state and above that a crossover to a spin ice state is seen before phase transitions to a charge ordered state and finally to a spin ordered state. The temperature at which the antiferromagnetic transition, spin ice crossover, and charge order transitions occur changes only slightly moving from $L = 1$ to $L = 4$. The biggest change from $L = 1$ to $L = 4$ is in the spin order transition. The temperature at which it occurs is heightened and moved much closer to the charge ordering peak.

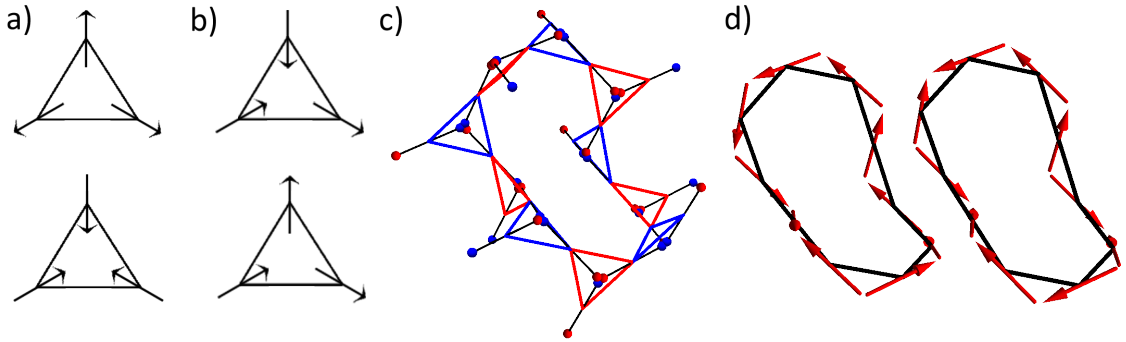

Figure 11: The four states that the hyperkagome lattice can access: a) The antiferromagnetic state, b) a spin ice state, c) a magnetic charge ordered state, and d) the spin ordered state.

Ordered States

The first transition for $J_{NN}/D_{NN} > -0.91$ is a transition to a charge ordered state. This state is one of ordered magnetic charges but disordered spins. On top of the spin ice restriction of two spins in,

one out or vice-versa neighbouring triangles will now always alternate between having two spins pointing towards the centre of the tetrahedra and two pointing away. This means that the average magnetic charge of neighbouring triangles will alternate between positive and negative.

A dumbbell model can also be used to explain this state as introduced by Castelnovo *et. al*(17). In the dumbbell model instead of vectors the spins are represented as dipoles with the separation between the poles such that they meet in the centre of the tetrahedron (see Fig. 10(c)). In the notation of this model neighbouring triangles will always have opposite average colour (commensurate with average magnetic charge).

The first investigation of the spin ordered state looked at the behaviour of the spins around the smallest loop that exists in the lattice. These loops nearly form rings of aligned or antialigned spins but always end up being "broken". The two ways this may occur are (see Fig. 11d) either with one spin around a loop of aligned spins pointing the wrong direction or two spins around a loop of antialigned spins aligning with their neighbouring spins in the loop. Looking further the aligned spins instead form long ferromagnetic chains through the lattice surrounding any antialigned chains, if they exist.

Simulations were also run upward in temperature from very low temperature starting from a configuration of the spins obtained from the original trials looking for hysteresis in the spin order transition peak. Hysteresis across a transition peak is one indicator that the transition might be of first order. No hysteresis was observed so, unlike in pyrochlore spin ice where the proposed ordering transition is known to be of first order(19), there is preliminary evidence that the ordering transition may not be first order.

Hyperkagome versus Pyrochlore Spin Ice

Given that the hyperkagome lattice forms from a diluted pyrochlore lattice and that we have studied a dipolar ice model with the same local $< 111 >$ axes it makes sense that there would be some similarities between dipolar ice models on these two lattices. The dipole-dipole interaction on pyrochlore was first treated by Siddharthan *et al.*(20) where the interaction was truncated at 5

nearest neighbours. They saw a sharp transition from paramagnetism to an ordered state in the region $J_{NN}/D_{NN} > -0.91$. This was disputed by Hertog *et al.*(18) who thought that the truncation was misleading and instead treated the problem using Ewald summation. Using Ewald summation they instead saw a broad smooth peak indicating a crossover to a spin ice state in the region of $J_{NN}/D_{NN} > -0.91$ and an antiferromagnetic transition for $J_{NN}/D_{NN} < -0.91$. Later a loop algorithm was constructed for the pyrochlore lattice that allowed them to see a transition to a magnetically ordered state after the spin ice crossover(19). The single transition to a magnetically ordered state instead of the two transitions as seen in hyperkagome comes from being a tetrahedral based lattice instead of triangular. On each tetrahedron in the spin ice state the average magnetic moment is 0 while in triangular based lattices the average magnetic moment is ± 1 allowing for magnetic interactions between triangles to create a transition intermediate to those seen on pyrochlore.

From the analytics for hyperkagome spin ice it was seen that the change from a single antiferromagnetic transition to a spin ice state happens at a value of $J_{NN}/D_{NN} \approx -0.91$. This is the same value as reported for pyrochlore spin ice(18). Both lattices also contain an antiferromagnetic transition and spin ice crossover whose shape as a function of J_{NN}/D_{NN} follows a qualitatively similar pattern and they both have an ordering transition that occurs at a value of T/D_{NN} that is independent of J_{NN}/D_{NN}. It should be noted though that although pyrochlore's antiferromagnetic transition occurs at a higher temperature than that of hyperkagome, hyperkagome's spin ice transition occurs at a higher temperature than that of pyrochlore. Also, both the charge and spin ordering transitions occur at higher temperatures than the ordering transition on pyrochlore. This may make it easier to access the low temperature features of hyperkagome spin ice than on pyrochlore spin ice due to the slightly heightened temperatures at which they occur.

Similarly a comparison could be made to spin ice on the kagome lattice(11), another pure $1/4$ non-magnetic impurity doping of the pyrochlore lattice. Although kagome is 2D and hyperkagome is 3D there are still several parallels to draw. The three transitions that occur in the region of $J_{NN}/D_{NN} > -0.91$ almost all have direct relations to the transitions seen on kagome. All three lattices, pyrochlore, hyperkagome, and kagome, see the first crossover to a spin ice state as well as

an ordering transition at low temperature but only hyperkagome and kagome see an intermediate state. In both cases it is a charge ordered state where the magnetic charges around the smallest loop that exists in the lattice alternate between average positive and average negative. The ordering transition between the two lattices is similar, namely they both try to form aligned/antialigned spins around the smallest loop, but ultimately hyperkagome finds it more energetically efficient to not form these loops while kagome doesn't.

Hyperkagome versus Garnet Spin Ice

The garnet lattice contains two interpenetrating lattices topologically equivalent to the hyperkagome lattice. Work done by Yoshioka *et al.*(40) on a local Ising model using both a nearest neighbour interaction and long range dipole-dipole interactions has shown similar results to those found here. They saw a spin ice crossover followed by an ordering transition at lower temperature. Loop algorithm Monte Carlo was not conducted in this work to be able to compare the possibility of multiple low temperature ordering transitions. Also, although the claim was made that long range dipole-dipole interactions were studied using Ewald summations and that they resulted in qualitatively similar heat capacity curves to those of truncated neighbour dipole-dipole interactions this data is not presented, only data for truncated neighbouring dipole-dipole interactions similar to what was done on kagome(11) is presented.

The garnet lattice of $Ho_3Ga_5O_{12}$(41) may be an extension of this work with two interpenetrating lattices topologically equivalent to the hyperkagome lattice. A first approximation of the properties of a spin ice garnet lattice could be made by mapping the spin structures found in this work for the hyperkagome lattice to garnet. Specifically in mapping them to the spatial coordinates of garnet in order to do static neutron scattering structure factor calculations for comparison with existing experimental neutron scattering data on this material(41).

It has been shown(42) that the unit cell of both hyperkagome and the two sublattices of garnet, as well as several other 3D, frustrated, triangular lattices, can be described by the locations given in Table IV through the use of the lattice parameter y. The nearest neighbour bond distance (d_{NN}) for

Site	Location
a	$\left(\frac{1}{8}, y, \frac{1}{4}+y\right)$
b	$\left(\frac{5}{8}, \frac{1}{2}-y, \frac{3}{4}-y\right)$
c	$\left(\frac{1}{4}-y, \frac{7}{8}, \frac{1}{2}+y\right)$
d	$\left(1-y, \frac{3}{4}+y, \frac{3}{8}\right)$
e	$\left(\frac{3}{8}, 1-y, \frac{3}{4}+y\right)$
f	$\left(\frac{1}{4}+y, \frac{1}{8}, y\right)$
g	$\left(\frac{3}{4}-y, \frac{5}{8}, \frac{1}{2}-y\right)$
h	$\left(\frac{1}{2}+y, \frac{1}{4}-y, \frac{7}{8}\right)$
i	$\left(\frac{7}{8}, \frac{1}{2}+y, \frac{1}{4}-y\right)$
j	$\left(\frac{3}{4}+y, \frac{3}{8}, 1-y\right)$
k	$\left(y, \frac{1}{4}+y, \frac{1}{8}\right)$
l	$\left(\frac{1}{2}-y, \frac{3}{4}-y, \frac{5}{8}\right)$

Table IV: The relative location of each spin within the unit cell.

each value of the lattice parameter y can be found from the minimum, non-zero distance between all sites within the unit cell. For the range of values shown in Fig. 12 the bond distance can be found using Eq. 14 with y bound between 0 and $\frac{1}{2}$. The two sublattices of the garnet lattice have values of the lattice parameter of $y = 0$ and $y = \frac{1}{2}$ while hyperkagome has a value of $y = \frac{1}{8}$.

$$d_{NN} = \begin{cases} y < 0.2 \text{ or } y = \frac{3}{8} & \sqrt{\left(\frac{1}{4}\right)^2 + \left(y+\frac{1}{8}\right)^2 + \left(y-\frac{1}{8}\right)^2} \\ y > 0.2 \text{ and } y \neq \frac{3}{8} & \sqrt{\left(y-\frac{3}{8}\right)^2 + \left(y-\frac{3}{8}\right)^2 + \left(2y-\frac{3}{4}\right)^2} \end{cases}, \tag{14}$$

Entropy

From the heat capacity the entropy remaining in an Ising spin system as a function of temperature can be calculated as:

$$\frac{S}{N}(T) = \ln 2 - \int_T^\infty \frac{C_V}{T} dT,$$

which is shown in Fig. 13 for several values of J_{NN}/D_{NN}. In order to approximate the summation in $T \to \infty$ the simulation was started at sufficiently high temperature such that $C_V = 0$. By fitting the curves locally around the inflection points with a seventh degree polynomial using computer

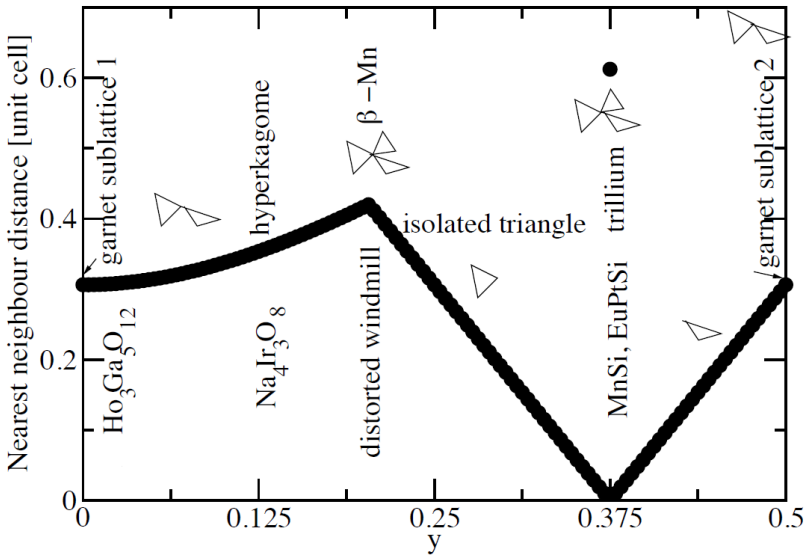

Figure 12: The nearest neighbour bond distance for a range of value of the lattice parameter y calculated from the minimum, non-zero value of the two bond distance formulas in Eq. 14. The trillium lattice is another corner-shared triangle based, three-dimensional, frustrated lattice but with each spin belonging to 3 triangles. Its residual entropy has been found(43) to be slightly smaller than that of hyperkagome at $\frac{S}{N} = \ln\frac{3}{2}$.

based fitting tools the residual entropy at which the inflection points exist can be calculated. The inflection point corresponding to the spin ice crossover gives a residual entropy of 0.502 ± 0.001 which is within error of the Pauling estimate of $\frac{1}{3}\ln\frac{9}{2}$. The inflection point for the charge ordered transition can also be calculated and is found to be 0.138 ± 0.001. Unlike the value obtained at the spin ice crossover we do not at the current time have an explanation for the value of this quantity as it is not a direct size scaling of the value expected at $L = 1$. Using $\frac{S}{N} = \frac{1}{N}\ln\Omega$ the degeneracy of this state was found to be approximately 10^{46} which, although large, is near 0% of both the total possible configurations of the lattice and the degeneracy of the spin ice state. At $L = 1$ the degeneracy of the charge ordered state was 18. This state does not appear to scale in size in a similar fashion as the spin ice crossover and spin ordering transition. The zero temperature residual entropy cannot be extracted from an inflection point. Instead it was done by looking at the configuration of the spins of all Monte Carlo trials run at $L = 4$ and noticing that there are 6 different configurations that can be found (3 unique configurations plus their inverses). These 6 configurations are identically the 6 configurations found in the ground state at $L = 1$ which are

shown in Table III. This, along with the entropy versus temperature plots tending towards this value as $T \to 0$, makes a strong case that the residual entropy of hyperkagome is $\frac{S}{N} = \frac{1}{N} \ln 6$ which will tend to zero for realistically large lattices.

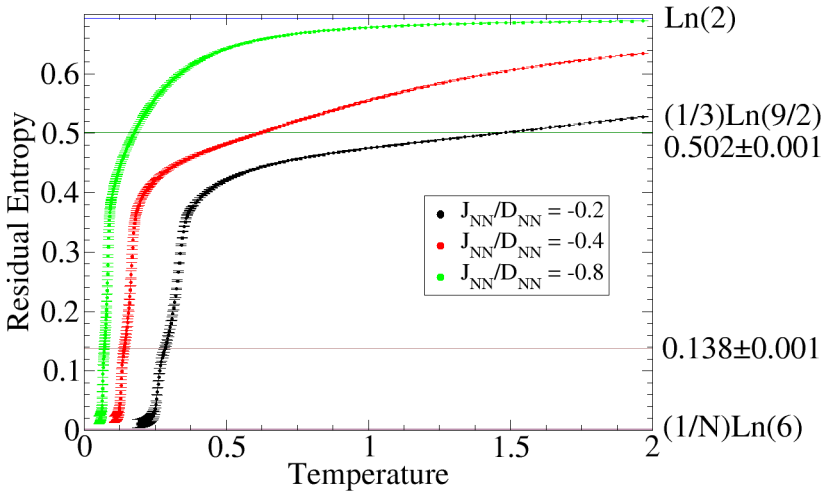

Figure 13: The residual entropy of the dipole-dipole interaction on the spin ice hyperkagome lattice.

Chapter IV: Conclusions

Hybrid single spin flip, loop algorithm Monte Carlo simulations of the dipolar spin ice model have been carried out on the hyperkagome lattice. Both an antiferromagnetic nearest neighbour interaction as well as a long range dipole-dipole interaction were simulated. This resulted in a phase diagram at $L = 4$ that is similar to that of the dipolar spin ice model on the pyrochlore lattice as previously studied by Melko *et al.*(19) in that a single transition to an antiferromagnetic ground state is seen for $J_{NN}/D_{NN} < -0.91$ and a crossover to a spin ice state followed by an ordering transition at low temperature was seen for $J_{NN}/D_{NN} > -0.91$. Such a transition has recently been found by Pomaranski *et al.*(44) who found that > 100 hours is required for equilibrium to be reached below the lowest temperature measured (0.34K). Unlike pyrochlore spin ice an intermediate transition to a charge ordered state is predicted on the hyperkagome lattice. This is reminiscent of what was seen for a dipolar spin ice model on the kagome lattice by Chern *et al.*(11) and comes about because of the difference in the average magnetic moment on a tetrahedron and triangle when in the spin ice state. Tetrahedra have an average magnetic moment of 0 in this state while for triangles the average magnetic moment is ± 1. This allows an additional ordering to take place between the average magnetic charges of each triangle.

The residual entropy estimate made for a random $1/4$ doping of the pyrochlore lattice is not equivalent to what is expected in the site ordered doping cases of kagome and hyperkagome. The assumption of a simple repulsion between neighbouring doped sites has been shown to resolve this issue. Such a repulsion may come about from distortions in the lattice if the non-magnetic atoms are of a different size than the magnetic ones. The site-ordering models that were created including such an onsite repulsion did not form any discussed lattice configuration nor was any short range repetition seen. So while this assumption will rectify the problem of the residual entropy of the purely random doping not matching that of the site ordered dopings it doesn't show that this would cause the doping to form on the hyperkagome lattice. Future investigations into further neighbour interactions between doped sites may provide a mechanism for the realization of a lattice that repeats over a short range like the hyperkagome lattice.

References

[1] L. Pauling, J. Am. Chem. Soc., **57** 2680 (1935).

[2] J.D. Bernal and R.H. Fowler, J. Chem. Phys. **1** (1933).

[3] P.W. Anderson, Mater. Res. Bull. **8**, 153-160 (1973).

[4] T.-H. Han, J.S. Helton, S. Chu, D.G. Nocera, J.A. Rodreguez-Rivera, C. Broholm and Y.S. Lee, Nature **492**, 406-410 (2012).

[5] J.G. Bednorz and K.A. Müller, Z. Physik B **64** (1986).

[6] P.W. Anderson, Science **235** 1196 (1987).

[7] W.F. Giauque and J.W. Stout, J. Am. Chem. Soc. **58**, 1144 (1936).

[8] M.J. Harris, S.T. Bramwell, D.F. McMorrow and T. Zeiske, K.W. Godfrey, Phys. Rev. Lett. **79** 2554 (1997).

[9] S. Rosenkranz, A.P. Ramirez, A. Hayashi, R.J. Cava, R. Siddharthan and B.S. Shastry, J. Appl. Phys. **87** 5914 (2000).

[10] A.S. Wills, R. Ballou and C. Lacroix, Phys. Rev. B **66** 144407 (2002).

[11] G.-Y. Chern, P. Mellado and O. Tchernyshyov, Phys. Rev. Lett. **106**, 207202 (2011).

[12] D.J.P. Morris, D.A. Tennant, S.A. Grigera, B. Klemke, C. Castelnovo, R. Moessner, C. Czternasty, M. Meissner, K.C. Rule, J.-U. Hoffmann, K. Keifer, S. Gerischer, D. Slobinsky and R.S. Perry, Science **326** 411 (2009).

[13] A.P. Ramirez, A. Hayashi, R.J. Cava, R. Siddharthan and B.S. Shastry, Nature **399** 333 (1999).

[14] S.T. Bramwell, M.J. Harris, B.C. den Hertog, M.J.P. Gingras, J.S. Gardner, D.F. McMorrow, A.R. Wildes, A.L. Cornelius, J.D.M. Champion, R.G. Melko and T. Fennell, Phys. Rev. Lett. **87** 047205 (2001).

[15] M. Kanada, Y. Yasui, Y. Kondo, S. Iikubo, M. Ito, H. Harashina, M. Sato, H. Okumura, K. Kakurai and H. Kadowaki, J. Phys. Soc. Jpn. **71** 313 (2002).

[16] S.V. Isakov, R. Moessner and S.L. Sondhi, Phys. Rev. Lett. **95** 217201 (2005).

[17] C. Castelnovo, R. Moessner, and S.L. Sondhi, Nature (London) **451**, 42 (2008).

[18] B.C. den Hertog and M.J.P. Gingras, Phys. Rev. Lett. **84** 3430 (2000).

[19] R.G. Melko and M.J.P. Gingras, J. Phys.: Condens. Matter **16**, R1277 (2004).

[20] R. Siddharthan, B.S. Shastry, A.P. Ramirez, A. Hayashi, R.J. Cava and S. Rosenkranz, Phys. Rev. Lett. **83** 1854 (1999).

[21] X. Ke, R.S. Freitas, B.G. Ueland, G.C. Lau, M.L. Dahlberg, R.J. Cava, R.Moessner, and P. Schiffer, Phys. Rev. Lett. **99**, 137203 (2007).

[22] R.D. Shannon, Acta Cryst. A32 pp. 751-767 (1976).

[23] L.D.C Jaubert and P.C.W. Holdsworth, Nature Phys. **5**, 256-261 (2009).

[24] S.T. Bramwell, S.R. Giblin, S. Calder, R. Aldus, D.Prabhakaran, and T. Fennell, Nature **461**, 956-959 (2009).

[25] Y. Qi, T. Brintlinger, and J. Cumings, Phys. Rev. B **77** 094418 (2008).

[26] P. Mellado, A. Concha, and L. Mahadevan, Phys. Rev. Lett. **109** 257203 (2012).

[27] L. Balents, Nature **464**, 199-208 (2010).

[28] M.P. Shores, E.A. Nytko, B.M. Bartlett, and D.G. Nocera, J. Am. Chem. Soc. **127** 13462 (2005).

[29] J.S. Helton, K. Matan, M.P. Shores, E.A. Nytko, B.M. Bartlett, Y. Yoshida, Y. Takano, A. Suslov, Y. Qiu, J.-H. Chung, D.G. Nocera, and Y.S. Lee, Phys. Rev. Lett. **98** 107204 (2007).

[30] M.A. de Vries, K.V. Kamenev, W.A. Kockelmann, J. Sanchez-Benitez, and A. Harrison, Phys. Rev. Lett. **100** 157205 (2008).

[31] See for example: Ref.11.

[32] M. Enjalran and M.J.P. Gingras, arXiv:cond-mat/0307151v1.

[33] The D_{ij} terms were computed by P. Carter for his undergraduate thesis under the supervision of Dr. M. Enjalran as suggested by Dr. J.M. Hopkinson.

[34] S. Kirkpatrick, C. D. Gelatt, M.P. Vecchi, Science **220** 671 (1983).

[35] N. Metropolis, A.W. Rosenbluth, M.N. Rosenbluth, A.H. Teller, and E. Teller, J. Chem. Phys. **21** 1087-1092 (1953).

[36] G.T. Barkema and M.E.J. Newman, Phys. Rev. E **57**, 1155 (1998).

[37] Private communications with Roger Melko at conference on Magn. Frust. Material (HFM June 2012).

[38] Y. Okamoto, M. Nohara, H. Aruga-Katori, and H. Takagi, Phys. Rev. Lett. **99** 137207 (2007).

[39] P. Carter, J.M. Hopkinson, and M. Enjalran, student talk (D13.00011) at APS March Meeting 2009, Mar. 16, 2009, unpublished.

[40] T. Yoshioka, A. Koga, and N. Kawakami, J. Phys. Soc. Jpn. **73** pp. 1805-1811 (2004).

[41] H.D. Zhou, C.R. Wiebe, L. Balicas, Y.J. Yo, Y. Qiu, J.R.D. Copley and J.S. Gardner, Phys. Rev. B **78**, 140406 (2008).

[42] S.V. Isakov, J.M. Hopkinson, and H.-Y. Kee, Phys. Rev. B **78** 014404 (2008).

[43] T.E. Redpath and J.M. Hopkinson, Phys. Rev. B **82** 014410 (2010).

[44] D. Pomaranski, L.R. Yaraskavitch, S. Meng, K.A. Ross, H.M.L Noad, H.A. Dabkowska, B.D. Gaulin, and J.B. Kycia, Nature Physics **9**, 353-356 (2013).

[45] P.P. Ewald, Ann. Physik **64**, 253 (1921).

Appendices

A. Ewald Summation

The dipole-dipole interaction energy $\mathscr{H}_{DD}$ depends on an infinte and conditionally convergent sum. In order to deal with this sum it is recast to two finite absolutely and rapidly convergent sums, one in real space and one in reciprocal space(45). The real space sum contains the short-range contribution to the interaction energy and the reciprocal space sum contains the long-range contribution. The dipole-dipole Hamiltonian of Eq. 3 can first be rewritten to remove the σ_i^α terms which are defined to be ± 1 as shown in Eq. 15. Ewald summation requires the system to be infinitely periodic with each repeated unit of the system referred to as a unit cell. One cell is used as the central cell and all others are referred to as mirrors of that cell.

$$\begin{aligned}\mathscr{H}_{DD} &= Dr_{NN}^3 \sum_{\substack{i>j \\ \alpha,\beta}} \left(\frac{\vec{s}_i^\alpha \cdot \vec{s}_j^\beta}{\left|\vec{r}_{ij}^{\alpha\beta}\right|^3} - \frac{3(\vec{s}_i^\alpha \cdot \vec{r}_{ij}^{\alpha\beta})(\vec{s}_j^\beta \cdot \vec{r}_{ij}^{\alpha\beta})}{\left|\vec{r}_{ij}^{\alpha\beta}\right|^5} \right) \\ &= Dr_{NN}^3 \sum_{\substack{i>j \\ \alpha,\beta}} \left(\frac{\hat{e}^\alpha \cdot \hat{e}^\beta}{\left|\vec{r}_{ij}^{\alpha\beta}\right|^3} - \frac{3\left(\hat{e}^\alpha \cdot \vec{r}_{ij}^{\alpha\beta}\right)\left(\hat{e}^\beta \cdot \vec{r}_{ij}^{\alpha\beta}\right)}{\left|\vec{r}_{ij}^{\alpha\beta}\right|^5} \right) \sigma_i^\alpha \sigma_j^\beta .\end{aligned} \tag{15}$$

Eq. 16 contains the real space contribution $\mathscr{R}_{ij}^{\alpha\beta}$ to the summation as calculated by Enjalran *et al.*(32). The sum in $\mathscr{R}_{ij}^{\alpha\beta}$ is between site i and site j in both the central unit cell as well as all mirrored unit cells. As such $\vec{r}_{ij}^{\alpha\beta} = \left(i_x L + R_{ij}^x, i_y L + R_{ij}^y, i_z L + R_{ij}^z\right)$ with L^3 being the number of 12 site hyperkagome unit cells within the Ewald unit cell and $\vec{R}_{ij}$ being a vector that points from site i to site j strictly within the central unit cell. This form of the vector simplifies the calculation of the effective neighbouring dipole-dipole interaction strengths.

$$\mathscr{R}_{ij}^{\alpha\beta} = \sum_{i_x,i_y,i_z} \left(\frac{\hat{e}^{\alpha}\cdot\hat{e}^{\beta}\,\mathrm{erfc}\left(\zeta\left|\vec{r}_{ij}^{\alpha\beta}\right|\right)}{\left|\vec{r}_{ij}^{\alpha\beta}\right|^{3}} + \frac{2\zeta\hat{e}^{\alpha}\cdot\hat{e}^{\beta}\mathrm{e}^{-\zeta^{2}\left|\vec{r}_{ij}^{\alpha\beta}\right|^{2}}}{\sqrt{\pi}\left|\vec{r}_{ij}^{\alpha\beta}\right|^{2}} - \frac{3\left(\hat{e}^{\alpha}\cdot\vec{r}_{ij}^{\alpha\beta}\right)\left(\hat{e}^{\beta}\cdot\vec{r}_{ij}^{\alpha\beta}\right)\mathrm{erfc}\left(\zeta\left|\vec{r}_{ij}^{\alpha\beta}\right|\right)}{\left|\vec{r}_{ij}^{\alpha\beta}\right|^{5}} - \frac{2\zeta\left(\hat{e}^{\alpha}\cdot\vec{r}_{ij}^{\alpha\beta}\right)\left(\hat{e}^{\beta}\cdot\vec{r}_{ij}^{\alpha\beta}\right)}{\sqrt{\pi}\left|\vec{r}_{ij}^{\alpha\beta}\right|^{4}}\left(3+2\zeta^{2}\left|\vec{r}_{ij}^{\alpha\beta}\right|^{2}\right)\mathrm{e}^{-\zeta\left|\vec{r}_{ij}^{\alpha\beta}\right|^{2}}\right). \tag{16}$$

The reciprocal space sum $\mathscr{D}_{ij}^{\alpha\beta}$ has been shown in Eq. 17 which was also done by Enjalran *et al.*(32). Here the sum is over reciprocal lattice vectors of the simple cubic simulation cell with $\vec{q} = \frac{2\pi}{L}(i_x, i_y, i_z)$. The reciprocal space sum contains a nonanalytic term at the point $\vec{q} = \vec{0}$. This term has been dropped from the calculation which doesn't effect the spin ice physics but may effect the ordered state in the case of $Tb_2Ti_2O_7$(32).

$$\mathscr{D}_{ij}^{\alpha\beta} = 4\pi \sum_{i_x,i_y,i_z} \frac{\left(\hat{e}^{\alpha}\cdot\vec{q}\right)\left(\hat{e}^{\beta}\cdot\vec{q}\right)}{|\vec{q}|^{2}} e^{-\frac{|\vec{q}|^{2}}{4\zeta^{2}}} \cos\left(\vec{q}\cdot\vec{r}_{ij}^{\alpha\beta}\right). \tag{17}$$

Both the real space and reciprocal space equations also contain a convergence parameter ζ that divides the weight of the dipole-dipole interaction summation between the two parts. The result of the summation is independent of the choice of ζ but its value determines the speed of convergence of each part. For this study a value of $\zeta = \frac{\sqrt{\pi}}{L}$ was used. This value made the real space and reciprocal space sums converge at roughly the same speed.

The code that computes the effective neighbouring dipole-dipole interaction strength works in two parts: one to calculate parameters of the lattice and a second to calculate the effective neighbouring dipole-dipole strenghts D_{ij}. The output of the lattice parameter calculator is a list of each site in the lattice at a given value of L along with its $<111>$ axis index (see Table II) and the site's vector offset within the lattice (see Table I).

The second part reads in the $\vec{r}_{ij}^{\alpha\beta}$ values computed in part one and uses them in the computation of the D_{ij} values. The results of this step are output into two separate files. The first file contains a

1st Nearest Neighbour	2nd Nearest Neighbour	3rd Nearest Neighbour
39.8493351153	−4.1887901563	−5.2190487659

Table V: The unique dipolar energies at $L = 1$.

j \ i	1	2	3	4	5	6	7	8	9	10	11	12
1		1	1	2	1	3	2	3	3	3	3	1
2			1	3	3	2	1	3	3	1	2	3
3				3	3	1	3	1	2	3	3	2
4					1	1	2	3	1	3	1	3
5						1	3	2	3	2	3	1
6							3	1	3	3	2	3
7								1	1	1	3	3
8									1	2	3	3
9										3	1	2
10											1	1
11												1
12												

Table VI: The index in the unique dipolar energy list (see table V) of each pair of spins i, j at $L = 1$.

list of unique D_{ij} values, one for each distance that two sites can be apart from one another within the bounds of the given lattice size. The second file contains a strictly upper diagonal matrix of indices into the file containing the D_{ij} values. The matrix needs only be strictly upper diagonal because the Hamiltonian sums sites with $i > j$.

The simulations loads both of these files into memory during startup. While computing the energy the index of each site at the given instance of the calculation is used to extract an index from the strictly upper diagonal matrix. This value can then be used to find the effective neighbouring energy D_{ij} and the calculation can proceed using the conventional Metropolis algorithm.

In simulations with only short range nearest neighbour interactions the checkboard algorithm can be used to decrease the run time of the simulations. It does this by splitting the lattice into two sublattices such that all sites in each sublattice can be updated simultaneously. This allows for easily scalable multiprocessing that can drastically decrease runtimes. When long range interaction such as the dipole-dipole interaction are involved this algorithm is not longer valid. Since an update of any spin in the lattice affects the energy of every other site in the lattice there is no way to split

the lattice into sublattices of any size other than 1. This means that simulations carried out with long range interactions are forced to mostly operate in series with much longer runtimes than potentially possible with short range interactions.